Research Article | Vol. 28, No. 23 / 9 November 2020 / Optics Express 34279
Optics EXPRESS

Upconversion detection of 1.25 Gb/s mid-infrared telecommunications using a silicon avalanche photodiode

ALAN C. GRAY,* SAM A. BERRY, LEWIS G. CARPENTER, JAMES C. GATES, CORIN B. E. GAWITH, AND PETER G. R. SMITH

Optoelectronics Research Centre, University of Southampton, University Road, Southampton, Hampshire, SO17 1BJ, UK
a.c.gray@soton.ac.uk

Abstract: With an ever-increasing interest in secure and reliable free-space optical communication, upconversion detectors enabled through nonlinear optical processes are an attractive route to transmitting data as a mid-infrared signal. This spectral region is known to have a higher transmissivity through the atmosphere. In this work, we present an upconversion scheme for detection in the silicon absorption band using magnesium-oxide doped periodically poled lithium niobate to generate 21 mW of a 3.4 μm signal from commercial laser sources using a difference frequency generation process. Following a further nonlinear frequency conversion, via sum-frequency generation, the resulting signal at 809 nm is detected. We achieve >50 μW of signal and bit error rates of 10^{-7} from a single-pass nonlinear conversion for both the transmitter and receiver systems without the need for additional optical amplifiers at the receiving end. The error rates due to potentially reduced laser powers at the receiver end are investigated and laser noise transfer through our system is discussed.

1. Introduction

As the majority of recent telecommunications research stretches towards high data transmission rates and reduction of errors through pioneering optical fibre technologies [1–3], development of free space optical (FSO) communication technologies remains an attractive route for communicating with unmanned aerial vehicles, high altitude platforms and satellites. This is alongside the abundance of bandwidth generated from multiplexing technologies [4–6]. FSO communication interests have also expanded into investigating LED modulation for indoor communications due to its viability to function as both lighting, data transmission and security [7]. Recent reviews of current FSO communication systems and research are presented by Willner *et al.* [8] and Son and Mao [9]. For FSO applications which require atmospheric transmission, the optimal spectral transmission windows have been shown to be between 3-5 μm and 8-12 μm [10,11]. However, readily available commercial laser sources, high-speed modulators and detectors are typically designed for operation at 1550 nm in the telecommunication C-band. Quasi-phasematched (QPM) crystals offer a tuneable, single frequency mid-IR (MIR) source given access to a tuneable source laser. Of these QPM technologies, magnesium-doped periodically poled lithium niobate (MgO:PPLN) is a natural choice of nonlinear crystal due to its high nonlinear coefficient, d_{33}, and transmission ranging from 400 nm to 5 μm and therefore enabling upconversion from MIR wavelengths; with early research in PPLN waveguides for MIR generation demonstrating its vast potential [12,13]. Given the transmission range of lithium niobate, the shorter-wave band for atmospheric transmission is more readily accessed.

#404855 https://doi.org/10.1364/OE.404855
Journal © 2020 Received 20 Aug 2020; revised 2 Oct 2020; accepted 5 Oct 2020; published 28 Oct 2020

Optics EXPRESS

Communication is not the only topic of interest for upconversion detection. Other popular applications areas include imaging [14–16], spectroscopy [17–19], LIDAR [20,21] and a recent demonstration of quantum interference at 2.1 μm [22]. Working in the MIR has potential benefits due to the $1/\lambda^4$ reduction in Rayleigh scattering from smaller particulates, and the ability to utilise the absorption spectrum of a particular gas, of which many molecules have interesting spectral features in this region due to their strong vibrational absorbance. Minimising the hindrance to communications via absorption from atmospheric gases and Mie scattering in adverse weather is also preferable [23]. Choosing a longer optical wavelength signal increases the associated correlation length, a parameter employed in numerically modelling the potential for free-space communications [24]. The enhanced security of data from malicious parties of the MIR signal is beneficial to the transmitting and receiving parties. This security arises due to the *a priori* knowledge of the specific MIR wavelength being required for detection. Recent research has shown promising capabilities for clearing atmospheric fog [25,26] and so a thorough understanding of the limitations in competing technologies is now required to converge upon an optimal communications scheme.

In this paper, we choose to implement well-established laser technologies to the task to investigate the conversion and transfer of data which has been superimposed on a MIR beam throughout our system. In contrast to previous telecommunications work in this area [27], we use sum-frequency generation (SFG) as the receiver process in which a visible/near-IR signal is created and detected; similar to the spectroscopic scheme presented by Wolf *et al.* [19]. With potentially high signal attenuation in FSO communications, higher quantum efficiency offered by silicon-based photodetectors than their InGaAs counterparts, alongside reduced dimensions and cost, make them a favourable detector option for MIR data transmission. The alternative spectral region for detection in this research means the communications data cannot be optically amplified using erbium-doped fibre amplifier (EDFA) technologies, and we must detect without amplification. In essence, we investigate the ability to reduce the number of components, and potentially weight and power consumption, of the receiver system by choosing detection in the silicon absorption band. This spectral band is likely to be a key area of future technological developments due single-photon experiments demonstrating lower timing jitter for high energy photons [28]. We demonstrate a 10^{-7} bit error ratio (BER) using this upconversion detection scheme and finally, we investigate the propagation of relative intensity noise from the pump lasers to the received signal.

2. Optical setup

We introduce the optical configuration, underlying theory and characterisation of the nonlinear components in this section. This comprises of a complete description of the transmitter and receiver components which are enabled through the DFG and SFG nonlinear processes, respectively. We utilise commercial lasers and re-use the pump laser as a means of reducing experimental complexity and cost of this system for both nonlinear optical processes. A schematic of this optical system is displayed in Fig. 1. To enable communications, the transmitter will generate the MIR beam with a pseudo-random bit stream (PRBS) superimposed in an amplitude modulation format, typically referred to as on-off keying (OOK). Fibre lasers offer near-perfect mode profiles with an M^2 close to unity, making this type of laser a highly-suitable choice for a nonlinear conversion applications; as such, beam shape need not be considered, unlike the application of diode lasers in nonlinear optics [29]. Our configuration uses a commercially available fiber laser at 1064 nm and a telecommunications C-band source which facilitates the OOK modulation scheme to be implemented. The optical configuration to realise the communications receiver will then comprise of a second nonlinear crystal and beam combination optics for the 1064 nm and MIR beams to carry out SFG. Both of these optical configurations and the nonlinear optical transmitting and receiving processes are discussed in the following sections.

Optics EXPRESS

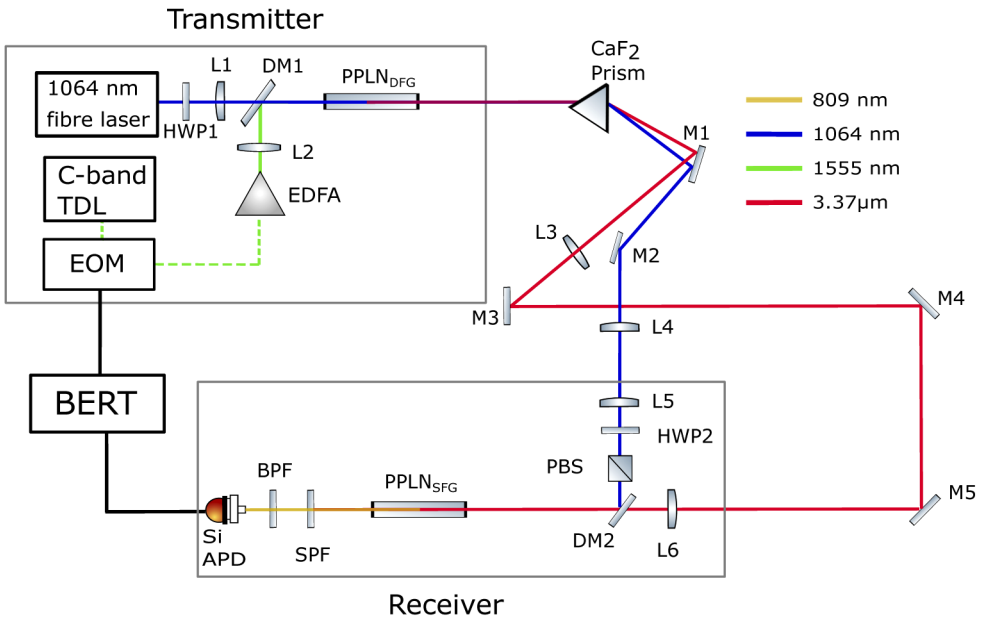

Fig. 1. Schematic of the optical setup. Solid, coloured lines represent a free-space optical beam, dashed coloured lines depict an optical fibre and solid black lines are electrical, RF cable connections.

2.1. *Down-conversion MIR generation: transmitter*

The 1064 nm laser used is a CW, linearly polarised, Yb-doped fibre laser with a 10 W maximum output (IPG photonics). We choose to rotate the polarisation using a half-wave plate (HWP1) rather than rotation of the fibre collimator as the delivery cable is armoured on our particular laser. The collimated beam is focused using a 150 mm lens, L1. The 1550 nm source is a 2 W, polarisation-maintaining EDFA (Keopsys) seeded with a <100 kHz linewidth, tuneable diode laser (TDL, Cobrite DX1). Given the typically high losses through a lithium niobate electro-optical modulator (EOM), this higher power C-band seed laser allows us to maintain a high signal to noise of the modulated C-band source for the nonlinear optical process and data transmission. The output from the EDFA is focussed using a 20 mm convex lens, L2. All lenses in this setup are AR coated for their respective wavelengths. The 1064 nm and modulated C-band lasers are combined using a short-pass dichroic mirror (DM1, Thorlabs DMSP1180). These beams are focussed into a 40 mm-long, MgO:PPLN crystal, supplied by Covesion Ltd. It is anti-reflected coated for the input wavelengths and from 2.6-4.8 μm in the MIR region with poling periods ranging from 29.52 to 31.59 μm. The crystal is housed in a PV40 oven (Covesion Ltd.) capable of 0.01 °C temperature stability from 30 to 200 °C.

As is common in the generation of MIR radiation, we use DFG as the nonlinear optical process in which the generated beam's wavelength, λ_3, is given by $1/\lambda_3 = 1/\lambda_1 - 1/\lambda_2$. In the case of DFG, the process is phasematched when

$$\Delta k_{\mathrm{DFG}} = k_{1064\ \mathrm{nm}} - k_{1555\ \mathrm{nm}} - k_{3.4\ \mu\mathrm{m}} - \frac{2\pi}{\Lambda} = 0, \tag{1}$$

where $k_i = 2\pi n_i/\lambda_i$ and Λ is the poling period of the QPM structure in PPLN$_{\mathrm{DFG}}$. The poling period to phasematch this nonlinear process was chosen using the Sellmeier coefficients by Gayer *et al.* [30]; the theoretical phasematching spectra in Figs. 2(a) and 3(a) also uses these coefficients. The Λ used in the DFG process used here is 30.49 μm.

Optics EXPRESS

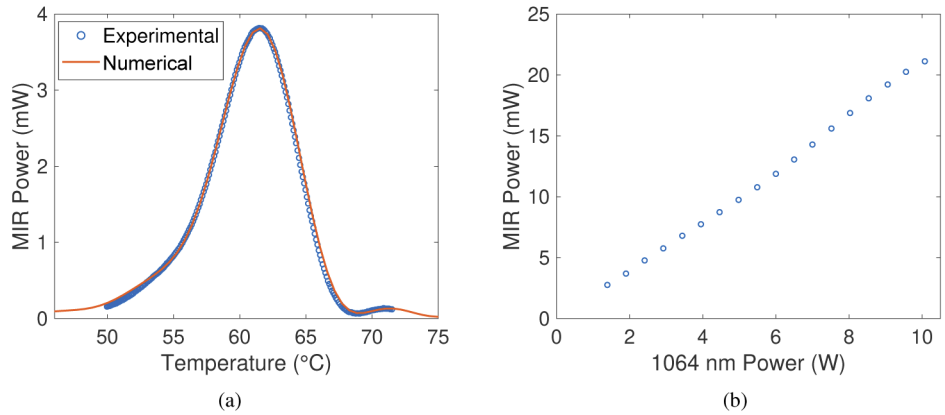

Fig. 2. (a) Temperature tuned phasematching curve for the DFG process and the associated theoretical spectrum, which is calculated using the commercial software SNLO, as discussed in the main text. (b) The power profile of our DFG process given a fixed 1550 nm power.

The plane-wave approximation which is usually presented in literature [19,31] for representing the relation of crystal length and input power to conversion efficiency is not appropriate for focussed Gaussian beams; where we allow the description of a tightly focussed beam to be defined by Smith [32], in which the Rayleigh range of the focussed beams is of the order of the crystal length. Tukker *et al.* [33] determined that in the focussed beam scenario, the power of the generated radiation via the DFG nonlinear process, $P_{3.4\ \mu m}$ is proportional to the following parameters as per

$$P_{3.4\ \mu m} \propto P_{1064\ nm} P_{1555\ nm} \frac{d_{eff}^2}{n_{1064\ nm} n_{1555\ nm} n_{3.4\ \mu m} \lambda_{3.4\ \mu m}^2} Lh \tag{2}$$

where L is the crystal length and h contains all parameters relevant to focussing conditions, as defined by Tukker *et al.* Hence, we simply provide a proportional relation here. We utilise the commercial software SNLO to theoretically analyse our system [34]. It was found that beam waists of 77 µm and 94 µm, for the 1064 nm and 1555 nm beams respectively, resulted in the best fit to our experimental phasematching curve, Fig. 2(a). The numerical phasematching spectrum is normalised to the experimental data for comparison.

As the aim is to minimise the loss in the generated MIR radiation, we use a calcium fluoride prism to separate the beams. Following separation, we use a protected silver mirror, M1, as it has lower absorption of the 1064 nm beam and an overall higher damage threshold than gold-plated reflectors. The 1064 nm beam is picked off using a dielectric mirror, M2. Mirrors M3, M4 and M5 only have incident MIR radiation; hence, these are MIR enhanced gold mirrors (Thorlabs, PF10-03-M02).

We characterise the generated power of the conversion process by maintaining the EDFA at 2 W and varying the 1064 nm power. The data presented in Fig. 2(b) was recorded on a thermal power meter (S302C, Thorlabs) with a broadband, AR-coated Ge window (WG91050-C9, Thorlabs) to filter any residual 1550 nm signal in the beam path post M3. A maximum MIR power of 21.1 mW was recorded, corresponding to an efficiency of 0.105%/W. The absorption of the Ge window at ~3.4 µm has been accounted for in the measured power. In comparison to similar single pass DFG works using these approximate wavelengths [27], this work is almost three times more efficient; generating 9.7 mW in comparison to 3.4 mW using 2 W (5 W) of the 1560 nm (1064 nm) source in our shorter crystal. This increase in efficiency is likely due to focussing conditions or preservation of polarisation. The higher power sources available in this

Optics EXPRESS

work are optimal for testing but the conversion efficiency is a key indicator for the potential to reduce the footprint of a transmitter source while still having enough power to reach the receiver. Theoretically, using SNLO, the maximum generated power will approach 54 mW (0.27%/W) for our system and estimated spot sizes. This model assumes a 14 pm/V d_{eff}, perfect overlap at the centre of the crystal and ideal M^2 values for both lasers. This is approximately ×2.5 more efficient than our current setup. Additionally, given these assumptions and parameters, a 30% decrease in spot size may lead to a 22% increase in generated MIR power. This lends weight to the hypothesis that this DFG process could be made more efficient in future work while still using commercial MgO:PPLN crystals.

2.2. Up-conversion visible/NIR generation: receiver

As previously mentioned, we choose to carry out the receiver process utilising SFG as the nonlinear optical process for photon conversion prior to measurement, also utilising PPLN as the $\chi^{(2)}$ nonlinear crystal. Prior to the mixing process, the residual 1064 nm pump beam is collimated and re-focussed using two 300 mm lenses, L4 and L5. The MIR beam is collimated post prism-separation using a 250 mm CaF_2 lens, L3. The MIR beam is then directed around an approximately 2 m length of space prior to focussing using a 200 mm lens, L6, and recombined with the 1064 nm beam via a dichroic mirror, DM2.

For the SFG process, PPLN_{SFG} is selected to satisfy

$$\Delta k_{\text{SFG}} = k_{1064\text{ nm}} + k_{3.4\text{ µm}} - k_{809\text{ nm}} + \frac{2\pi}{\Lambda} = 0. \tag{3}$$

where the generated wavelength is $1/\lambda_3 = 1/\lambda_1 + 1/\lambda_2$. In our case, the generated beam has a wavelength of 809 nm, and hence, falls within a silicon detector's responsivity spectrum. Our design beam waists in PPLN_{DFG} are ~80 µm and ~150 µm for the 1064 nm and MIR beams respectively. Due to the much larger MIR waist size, we assume a plane-wave description of this interaction. The generated power of the SFG process for weak signal mixing in the plane-wave regime is given by [32]

$$P_{809\text{ nm}} \propto \frac{P_{1064\text{ nm}} P_{3.4\text{ µm}}}{n_{1064\text{ nm}} n_{809\text{ nm}} n_{3.4\text{ µm}}} L^2 d_{\text{eff}}^2 \text{sinc}^2\left(\frac{\Delta k_{\text{SFG}} L}{2}\right), \tag{4}$$

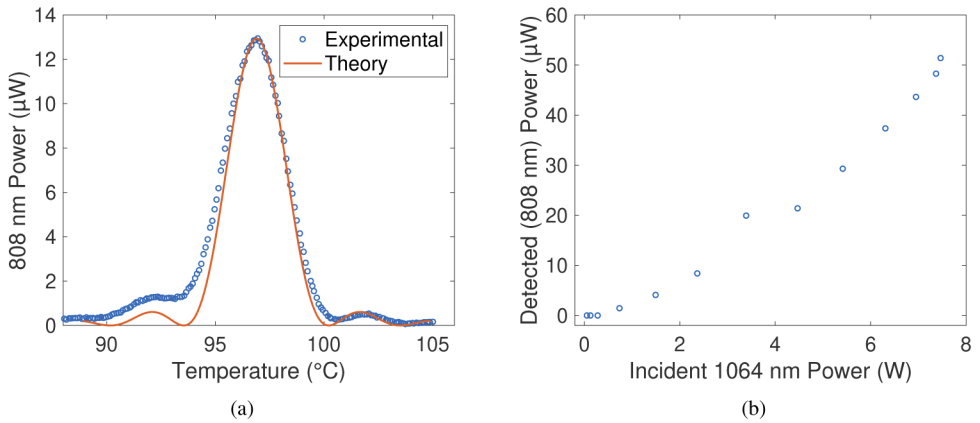

(a) (b)

Fig. 3. (a) Experimental SFG phasematching spectrum of PPLN_{SFG} alongside the theoretical spectrum. (b) The power response given a fixed MIR input and the re-used 1064 nm power being varied. Note that the 1064 nm power in the transmitter/DFG stage was kept constant for figure b).

Optics EXPRESS

where the conversion process is linearly dependent on either input power up until the photon flux limitation requires consideration. The characteristic quadratic dependence on the length of crystal is a feature of the plane-wave assumption. To perform this process, $PPLN_{SFG}$ is a 40 mm-long crystal with a period of 22.4 µm, also housed in a PV40 oven and is AR coated for both the input and generated frequencies.

Following the SFG conversion, a 900 nm short-pass filter (SPF) and a band pass filter (BPF) with a 40 nm transmission window centred at 800 nm are implemented prior to detection. The BPF's primary function is to filter the generated radiation from parasitic nonlinear processes; specifically, green light from second-harmonic generation of the 1064 nm source. The 809 nm signal is then fibre-coupled using a 20× microscope objective lens and a 1 m multi-mode optical fibre. The output is directed towards a large area silicon photodiode (S120C, Thorlabs) for power measurements. The phasematching curve for this conversion process is presented in Fig. 3(a). The theoretical curve assumes a plane-wave interaction and the minor differences in comparison to the experimental data is assumed to be due to non-ideal optical alignment and/or loose focussing conditions. The 1064 nm source is calibrated for loss from optical components to determine the power present at the facet of $PPLN_{DFG}$ and varied using HWP2 in combination with the polarising beam splitter (PBS). This calibration is performed using a thermal power meter (S302C, Thorlabs) and the 1064 nm laser set at ~2 W to operate within the detector's range. The relation in Eq. (4) predicts a linear relation to power. The nonlinear curve observed in Fig. 3(b) will be investigated in future work but it is predominantly due to the heating of the PPLN crystal and slight modification of the phasematching temperature for the SFG process.

Nevertheless, ~50 µW provides enough power for detection using a silicon avalanche photodiode for optical data transfer. Using these high-quality commercial sources, the optical conversion

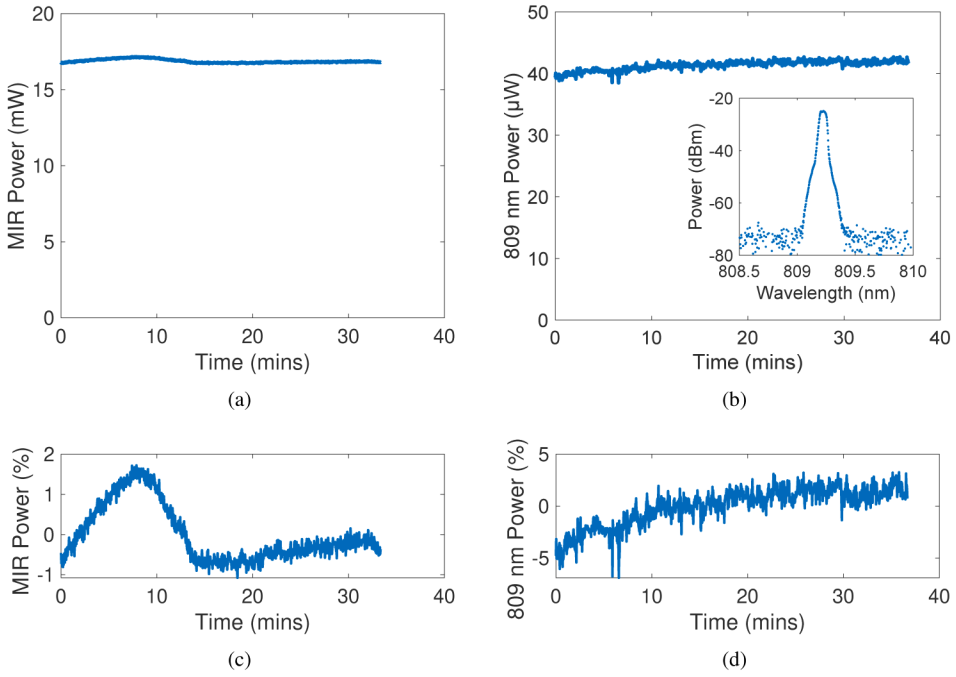

Fig. 4. Stability of generated signal after each nonlinear conversion process: (a) MIR beam as part of the transmitter and (b) near-IR beam after SFG with the previously generated MIR signal. The inset shows the spectrum of the generated 809 nm beam. (c) and (d) are the MIR and near-IR stability, respectively, represented as a percentage to the mean power observed.

Optics EXPRESS

scheme demonstrated intensity stability with standard deviations of 37 μW and 0.67 μW, over a 30-minute window, for the generated MIR and 809 nm signal, respectively. This data is presented in Figs. 4(a) and 4(b). The respective deviations as a percentage from the mean power are presented in Figs. 4(c) and 4(d). The DFG system and associated optical components are seen to reach thermal equilibrium after ∼15 mins. We also confirm at least a 45 dB signal-to-noise ratio for the generated 809 nm signal without any additional spectral filters whilst using commercial sources; thus establishing the potential for stable optical communications. Also, the 809 nm spectrum from the SFG does not show any detectable artefacts from a thermal background or spontaneous parametric downconversion.

3. Telecommunication results

In order to demonstrate the ability to transmit telecommunications information via conversion to and from the MIR, a bit error rate tester (BERT) is used to quantify the quality of data transmission in our current system. This BERT operates in a non-return to zero (NRZ) configuration. As the silicon detector used as part of the receiver was intentionally chosen to characterise the system when converting to the near-IR regime, a back-to-back measurement cannot be carried out. We select 1.25 GHz as the modulation frequency as it is an optimal compromise between the chosen modulation and detection equipment utilised. We used a silicon avalanche photodiode (APD, Menlosystems APD210) for BER measurements following the entirety of the upconversion detection system presented in Fig. 1. This detector has a maximum bandwidth of 1.6 GHz. An alternative to the APD technologies would be a GaAs PIN device which would offer >10GHz bandwidth, and opens prospects for much higher capacity links in future works where higher optical powers are attained at the detection wavelength.

Operating at the maximum MIR power output from our transmitter system, ∼ 21.1 mW, we explore the impact on BER as a function of the generated 809 nm light from the SFG process. To do this, the 1064 nm power is varied using HWP2, as previously described. We achieve a minimum BER of 1.1×10^{-7}, as presented in Fig. 5(a). The corresponding 1064 nm power at the input facet of $PPLN_{SFG}$ is shown in Fig. 5(b), of which the power at the laser source was held constant at 10 W. The measured BER is somewhat constant from 20 μW to 50 μW. We anticipate this is due to the current modulation components in use as overshoot can be seen in Fig. 6(a). We expect a minor amount of this is attributed to the RF amplifier required to drive the EOM correctly following the output signal from the BER. This is likely the current limitation in further reduction of the BER value as this is not an inherent nonlinear optical property; offering further routes for improvement in future work. However, the modulated data continues to show a clear eye opening for reduced powers and higher BERs, Fig. 6(b). For their OOK data transmission results, Su *et al.* achieve BERs approaching 10^{-10}. With these improvements, we anticipate the BER of our system will reduce towards this range.

Due to the chosen method of re-using the pump beam, we confirmed the transfer of data is not a result of pump depletion on the 1064 nm beam by rotating the polarisation of the beam 45 degrees at HWP1. The type-0 nonlinear interaction used here utilises only the extraordinary polarisation present in the crystal, the vector component which is now 90 degrees rotated away from the correct polarisation will now be unused, i.e., there is no possibility of depletion; the MIR power is reduced to 9.2 mW, approximately half of the power recorded directly prior to the polarisation rotation, as expected. Subsequently, HWP2 was arranged to rotate the polarisation by a further 90 degrees to use the orthogonal polarisation vector. A 14.5 μW power of 809 nm light was detected with a BER of 3.6×10^{-5}, which corresponds to a similar value of that obtained for this power level with the original polarisation arrangement of the 1064 nm beam.

Optics EXPRESS

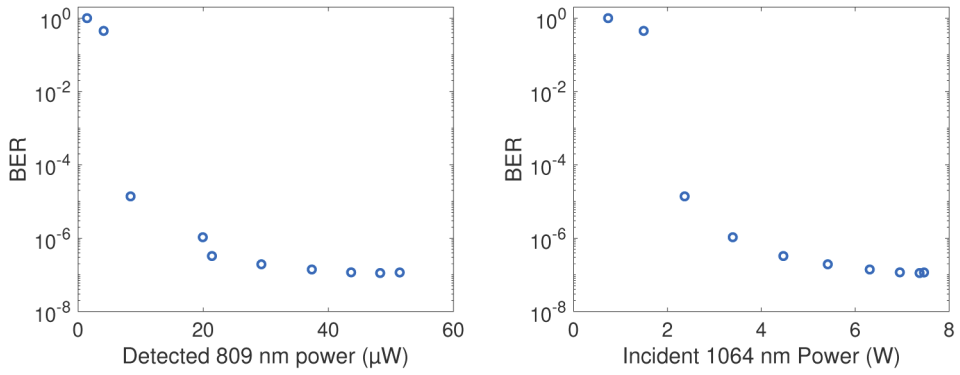

Fig. 5. Rotating HWP2 to investigate the receiver system. (a) 809 nm power detected on the APD and the corresponding BER value. (b) BER as a function of the 1064 nm power incident on PPLN_{SFG}.

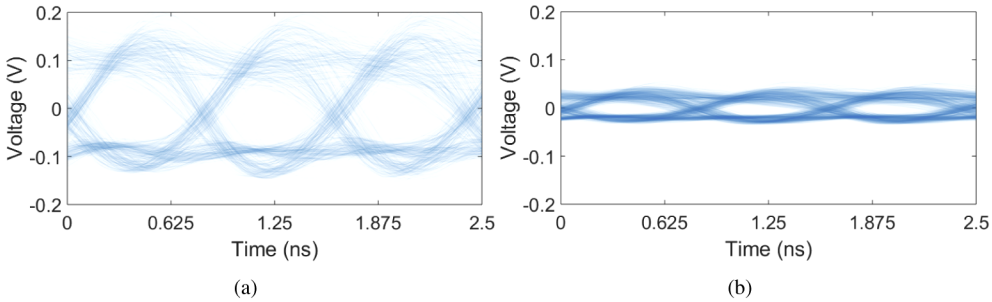

Fig. 6. Eye diagrams recorded for (a) the lowest BER achieved and (b) a BER of approximately 10^{-5}.

4. Transfer of relative intensity noise

To comment on the transfer of noise throughout this system, we use a methodology and mathematical notation similar to that presented by Tawfieq *et al.* [35]. The power spectral density (PSD), $S_p(f)$, of the associated noise characteristics of the laser is

$$S_p(f)[\text{dBc/Hz}] = S_p(f)[\text{dBm/Hz}] - 10\log_{10}\left(\frac{V^2}{R_S G}\right) \tag{5}$$

where V is the DC voltage of the carrier signal, R_S is the source impedance and G is the relative gain between the DC and AC components of the electrical signal due to our choice of detectors which have an internal bias-tee prior to amplification. Thence, V is measured at the DC output of the detector and is not assumed based on knowledge of the responsivity of the semiconductor material. The detectors used are New Focus photoreceivers, models 1601 and 1611, with a silicon and InGaAs absorption spectrum, respectively. In our case, the data from the RF spectrum analyser is given as dBm and is post-processed in order to scale it correctly to dBm/Hz. Our electronic components are all 50 Ω impedance matched.

Comparing relative intensity noise (RIN), or any related noise parameter, is notoriously challenging when the experiment requires a variety of detectors with different absorption profiles. Typically, the DC current or CW optical power imparted on the photodetector is a constant across the experimental lasers sources in an effort to simplify the calculation of the carrier signal. In this

Optics EXPRESS

work, we only wish to investigate the propagation of noise, and not the absolute RIN level. Hence, the presented noise spectra in Fig. 7 are the result of calibrating for variance in responsivity, taken from [36], for the relevant detector with respect to noise frequency. This final step is due to the changing optical-to-electronic parameters typically discussed in RIN calculations. Also, the varying shot noise, which would result from the consequential DC current generated [37], may play a role in the overall curve of the noise spectra due to the low powers available here for characterisation of the 809 nm signal.

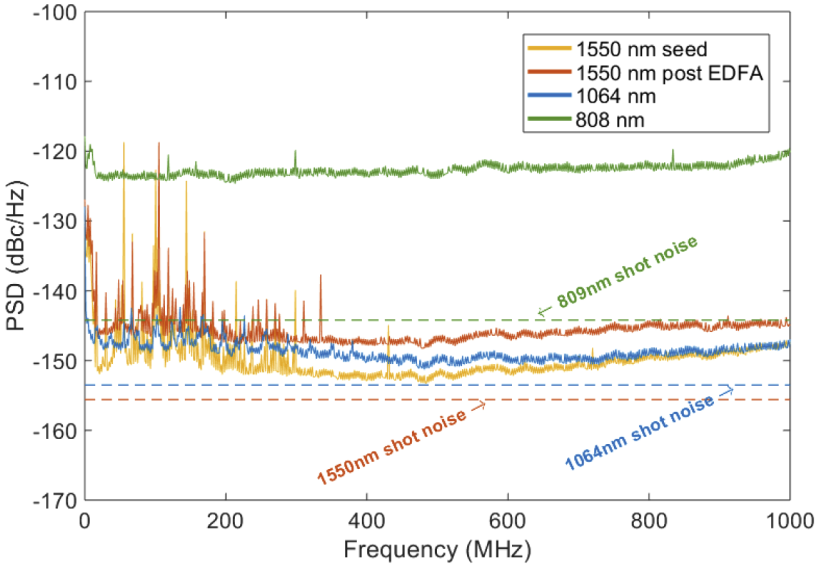

Fig. 7. Power spectral density of the noise associated to each laser used in the upconversion detector along with the generated 809 nm beam and related shot noise levels. The shot noise level of the 809 nm beam is substantially higher due to the limited power generated in the single-pass, bulk PPLN configuration.

Unlike previous works [35], we offer a qualitative discussion of noise level. To analyse the contribution of intensity noise in our system, we firstly exchange the EDFA used in previous discussions to a higher power version with a maximum output of 5 W to increase the average 809 nm optical power to 129 μW. Our system comprises a single contribution from the 1550 nm source and two contributions from the 1064 nm fibre laser and a path length difference between the generated MIR beam and the second interaction. The dense population of peaks in the noise signals under 300 MHz are typically a result of electrical noise and the power supplies used to power the laser sources. Sufficiently far away from these noise peaks, at 800 MHz the generated 809 nm signal's noise is approximately 22.5 dB above its shot noise limit, σ, where we define this as

$$\sigma_i = S_p, i(f) - \sigma_{shot,i}. \tag{6}$$

We hypothesise/propose this level of noise is a result of the contributing source lasers to the final SFG process, i.e., $2\sigma_{1064} + \sigma_{1550}$, which equals ~ 22 dB in our case. Performing this calculation at the higher frequency enables working beyond the correlation time of the noise due to our path length difference in the beams, thus we can assume the noise sources are random and independent. As laser RIN is a relevant factor for spectroscopy applications, considering the contributing noise sources is vital prior to system development if applications were to employ a scheme in which the pump is re-used rather than split before the nonlinear processes. Our work here indicates an equal contribution of excess spectral noise relative to the shot noise floor

Optics EXPRESS

per each pass through a nonlinear process, implying the 1064 nm source may be worth more consideration when designing a system that uses this source twice.

5. Conclusion

We have characterised an upconversion detection system designed for telecommunications transmission of a MIR, amplitude modulated signal to investigate the applicability of detection in the silicon absorption band. This was carried out using commercially available laser sources, PPLN crystals and a silicon APD. We achieve a minimum BER of 10^{-7} for transmission of 1.25 Gbps data in an on-off keying modulation format where no further optical amplification has been implemented to boost the signal prior to detection; in doing so, we examine the applicability for using fewer components in free-space communications of MIR signals. We also investigated the noise contributions from the relevant lasers in the presented optical configuration and postulated the contribution source of each laser used. This has been achieved using single-pass nonlinear conversion in bulk crystals and component limitations have been identified. Future work in this area is primarily expected to take the form of waveguide development for enhanced conversion efficiency and miniaturisation.

Funding

Air Force Office of Scientific Research (FA9550-16-1-0531); Engineering and Physical Sciences Research Council (EP/M013243/1, EP/M013294/1, EP/M024539/1, EP/T00097X/1); Innovate UK (102805, 104000, 104613).

Acknowledgments

We would like to thank Dr. Jonathan Woods for the loan of an RF spectrum analyser.

Disclosures

The authors declare no conflicts of interest.

References

1. G. Rademacher, R. S. Luís, B. J. Puttnam, T. A. Eriksson, R. Ryf, E. Agrell, R. Maruyama, K. Aikawa, Y. Awaji, H. Furukawa, and N. Wada, "High capacity transmission with few-mode fibers," J. Lightwave Technol. **37**(2), 425–432 (2019).
2. Z. Liu, B. Karanov, L. Galdino, J. R. Hayes, D. Lavery, K. Clark, K. Shi, D. J. Elson, B. C. Thomsen, M. N. Petrovich, D. J. Richardson, F. Poletti, R. Slavik, and P. Bayvel, "Nonlinearity-free coherent transmission in hollow-core antiresonant fiber," J. Lightwave Technol. **37**(3), 909–916 (2019).
3. Y. Chen, Z. Liu, S. R. Sandoghchi, G. T. Jasion, T. D. Bradley, E. N. Fokoua, J. R. Hayes, N. V. Wheeler, D. R. Gray, B. J. Mangan, R. Slavík, F. Poletti, M. N. Petrovich, and D. J. Richardson, "Multi-kilometer long, longitudinally uniform hollow core photonic bandgap fibers for broadband low latency data transmission," J. Lightwave Technol. **34**(1), 104–113 (2016).
4. J. Wang, J.-Y. Yang, I. M. Fazal, N. Ahmed, Y. Yan, H. Huang, Y. Ren, Y. Yue, S. Dolinar, M. Tur, and A. Willner, "Terabit free-space data transmission employing orbital angular momentum multiplexing," Nat. Photonics **6**(7), 488–496 (2012).
5. G. Milione, M. P. Lavery, H. Huang, Y. Ren, G. Xie, T. A. Nguyen, E. Karimi, L. Marrucci, D. A. Nolan, R. R. Alfano, and A. E. Willner, "4× 20 Gbit/s mode division multiplexing over free space using vector modes and a q-plate mode (de) multiplexer," Opt. Lett. **40**(9), 1980–1983 (2015).
6. H. Huang, G. Xie, Y. Yan, N. Ahmed, Y. Ren, Y. Yue, D. Rogawski, M. J. Willner, B. I. Erkmen, K. M. Birnbaum, S. J. Dolinar, M. P. J. Lavery, M. J. Padgett, M. Tur, and A. E. Willner, "100 Tbit/s free-space data link enabled by three-dimensional multiplexing of orbital angular momentum, polarization, and wavelength," Opt. Lett. **39**(2), 197–200 (2014).
7. H. Chun, A. Gomez, C. Quintana, W. Zhang, G. Faulkner, and D. O'Brien, "A wide-area coverage 35 Gb/s visible light communications link for indoor wireless applications," Sci. Rep. **9**(1), 4952 (2019).
8. A. E. Willner, Y. Ren, G. Xie, Y. Yan, L. Li, Z. Zhao, J. Wang, M. Tur, A. F. Molisch, and S. Ashrafi, "Recent advances in high-capacity free-space optical and radio-frequency communications using orbital angular momentum multiplexing," Philos. Trans. R. Soc., A **375**(2087), 20150439 (2017).

Optics EXPRESS

9. I. K. Son and S. Mao, "A survey of free space optical networks," Digit. Commun. Netw.. **3**(2), 67–77 (2017).
10. T. Plank, E. Leitgeb, P. Pezzei, and Z. Ghassemlooy, "Wavelength-selection for high data rate free space optics (FSO) in next generation wireless communications," in *17th European Conference on Networks and Optical Communications*, (IEEE, 2012), pp. 1–5.
11. A. Rogalski and K. Chrzanowski, "Infrared devices and techniques," Optoelectronics Review **10**, 111–136 (2002).
12. M. Asobe, O. Tadanaga, T. Yanagawa, T. Umeki, Y. Nishida, and H. Suzuki, "High-power mid-infrared wavelength generation using difference frequency generation in damage-resistant Zn:$LiNbO_3$ waveguide," Electron. Lett. **44**(4), 288–290 (2008).
13. K.-D. F. Büchter, H. Herrmann, C. Langrock, M. M. Fejer, and W. Sohler, "All-optical Ti:PPLN wavelength conversion modules for free-space optical transmission links in the mid-infrared," Opt. Lett. **34**(4), 470–472 (2009).
14. Q. Zhou, K. Huang, H. Pan, E. Wu, and H. Zeng, "Ultrasensitive mid-infrared up-conversion imaging at few-photon level," Appl. Phys. Lett. **102**(24), 241110 (2013).
15. J. S. Dam, P. Tidemand-Lichtenberg, and C. Pedersen, "Room-temperature mid-infrared single-photon spectral imaging," Nat. Photonics **6**(11), 788–793 (2012).
16. R. Demur, R. Garioud, A. Grisard, E. Lallier, L. Leviandier, L. Morvan, N. Treps, and C. Fabre, "Near-infrared to visible upconversion imaging using a broadband pump laser," Opt. Express **26**(10), 13252–13263 (2018).
17. Q. Hu, J. S. Dam, C. Pedersen, and P. Tidemand-Lichtenberg, "High-resolution mid-IR spectrometer based on frequency upconversion," Opt. Lett. **37**(24), 5232–5234 (2012).
18. P. Tidemand-Lichtenberg, J. S. Dam, H. Andersen, L. Høgstedt, and C. Pedersen, "Mid-infrared upconversion spectroscopy," J. Opt. Soc. Am. B **33**(11), D28–D35 (2016).
19. S. Wolf, T. Trendle, J. Kiessling, J. Herbst, K. Buse, and F. Kühnemann, "Self-gated mid-infrared short pulse upconversion detection for gas sensing," Opt. Express **25**(20), 24459–24468 (2017).
20. L. Høgstedt, A. Fix, M. Wirth, C. Pedersen, and P. Tidemand-Lichtenberg, "Upconversion-based lidar measurements of atmospheric CO_2," Opt. Express **24**(5), 5152–5161 (2016).
21. M. Widarsson, M. Henriksson, P. Mutter, C. Canalias, V. Pasiskevicius, and F. Laurell, "High resolution and sensitivity up-conversion mid-infrared photon-counting LIDAR," Appl. Opt. **59**(8), 2365–2369 (2020).
22. S. Prabhakar, T. Shields, A. C. Dada, M. Ebrahim, G. G. Taylor, D. Morozov, K. Erotokritou, S. Miki, M. Yabuno, H. Terai, C. B. E. Gawith, M. Kues, L. Caspani, R. H. Hadfield, and M. Clerici, "Two-photon quantum interference and entanglement at 2.1 μm," Sci. Adv. **6**(13), eaay5195 (2020).
23. W. O. Popoola and Z. Ghassemlooy, "BPSK subcarrier intensity modulated free-space optical communications in atmospheric turbulence," J. Lightwave Technol. **27**(8), 967–973 (2009).
24. X. Zhu and J. M. Kahn, "Free-space optical communication through atmospheric turbulence channels," IEEE Trans. Commun. **50**(8), 1293–1300 (2002).
25. M. C. Schroeder, I. Larkin, T. Produit, E. W. Rosenthal, H. Milchberg, and J.-P. Wolf, "Molecular quantum wakes for clearing fog," Opt. Express **28**(8), 11463–11471 (2020).
26. A. Rudenko, P. Rosenow, V. Hasson, and J. V. Moloney, "Plasma-free water droplet shattering by long-wave infrared ultrashort pulses for efficient fog clearing," Optica **7**(2), 115–122 (2020).
27. Y. Su, W. Wang, X. Hu, H. Hu, X. Huang, Y. Wang, J. Si, X. Xie, B. Han, H. Feng, Q. Hao, G. Zhu, T. Duan, and W. Zhao, "10 Gbps DPSK transmission over free-space link in the mid-infrared," Opt. Express **26**(26), 34515–34528 (2018).
28. B. Baek, K. S. McKay, M. J. Stevens, J. Kim, H. H. Hogue, and S. W. Nam, "Single-photon detection timing jitter in a visible light photon counter," IEEE J. Quantum Electron. **46**(6), 991–995 (2010).
29. A. K. Hansen, M. Tawfieq, O. B. Jensen, P. E. Andersen, B. Sumpf, G. Erbert, and P. M. Petersen, "Concept for power scaling second harmonic generation using a cascade of nonlinear crystals," Opt. Express **23**(12), 15921–15934 (2015).
30. O. Gayer, Z. Sacks, E. Galun, and A. Arie, "Temperature and wavelength dependent refractive index equations for MgO-doped congruent and stoichiometric $LiNbO_3$," Appl. Phys. B **91**(2), 343–348 (2008).
31. R. L. Sutherland, *Handbook of nonlinear optics* (CRC press, 2003).
32. A. V. Smith, *Crystal nonlinear optics: with SNLO examples* (AS-Photonics, 2018).
33. T. W. Tukker, C. Otto, and J. Greve, "Elliptical-focusing effect on parametric oscillation and downconversion," J. Opt. Soc. Am. B **15**(9), 2455–2461 (1998).
34. A. Smith, "SNLO software package," www.as-photonics.com (2008).
35. M. Tawfieq, A. K. Hansen, O. B. Jensen, D. Marti, B. Sumpf, and P. E. Andersen, "Intensity noise transfer through a diode-pumped titanium sapphire laser system," IEEE J. Quantum Electron. **54**(1), 1–9 (2018).
36. "Optical receiver, 320-1000 nm silicon detector, 30 kHz to 1 GHz Bandwidth," https://www.newport.com/p/1601FS-AC.
37. P. Horowitz, "The art of electronics–3rd edition," Horowitz W. Hill–NY.: Cambridge University, 1192 p (2015).